# R3GAN-based Optimal Strategy for Augmenting Small Medical Datasets

Tsung-Wei Pan
Department of Electrical Engineering
National Taiwan Ocean University
Keelung 202301, Taiwan
well90111829@gmail.com

Ming-Jer Chen
Department of Obstetrics, Gynecology
and Woman's Health, TVGH, 407219
Taichung
mingjerchen@gmail.com

Chang-Hong Wu
Department of Electrical Engineering
National Taiwan Ocean University
Keelung 202301, Taiwan
s0979979782@gmail.com

Yu-Chiao Yi Department of Obstetrics, Gynecology and Woman's Health, TVGH, 407219 Taichung yuchiaoyi@gmail.com Jung-Hua Wang\*
AI Research Center
National Taiwan Ocean University
Keelung 202301
jhwang@email.ntou.edu.tw

Tsung-Hsien Lee
Department of Obstetrics and
Gynecology, Chung Shan Medical
University Hospital, Taichung 40201,
Taiwan
jackth.lee@gmail.com

Abstract—Medical image analysis often suffers from data scarcity and class imbalance, limiting the effectiveness of deep learning models in clinical applications. Using human embryo time-lapse imaging (TLI) as a case study, this work investigates how generative adversarial networks (GANs) can be optimized for small datasets to generate realistic and diagnostically meaningful images. Based on systematic experiments with R3GAN, we established effective training strategies and designed an optimized configuration for 256×256-resolution datasets, featuring a full burn-in phase and a low, gradually increasing  $\gamma$  range (5  $\rightarrow$  40). The generated samples were used to balance an imbalanced embryo dataset, leading to substantial improvement in classification performance. The recall and F1score of t3 increased from 0.06 to 0.69 and 0.11 to 0.60, respectively, without compromising other classes. These results demonstrate that tailored R3GAN training strategies can effectively alleviate data scarcity and improve model robustness in small-scale medical imaging tasks.

Keywords—R3GAN, medical image generation, small dataset training, embryo time-lapse imaging, data augmentation

# I. INTRODUCTION

In recent years, machine learning (ML) techniques have demonstrated significant promise in the medical domain, particularly for clinical diagnosis and decision-making through medical image analysis. These data-driven approaches leverage advancements in computer vision to enhance the consistency and reliability of clinical assessments. Despite this potential, the development of robust medical ML models faces a critical obstacle: data scarcity and heterogeneity. Unlike large-scale natural image datasets (e.g., ImageNet), medical data acquisition is severely constrained by ethical and privacy regulations (e.g., HIPAA [1] and GDPR [2]), limiting large-scale sharing. Furthermore, expert annotation is costly and time-consuming, and certain conditions are characterized by biological rarity and temporal specificity, which further restrict the availability of representative samples. This inherent data limitation poses a fundamental challenge to the stability and performance of deep learning models.

A representative example is the time-lapse imaging (TLI) of human embryos. TLI continuously records embryo development from fertilization to the blastocyst stage, providing valuable morphological information for embryologists. However, certain developmental transitions, such as the two-cell to four-cell division, are highly transient. The three-cell (t3) stage, which occurs between these divisions,

lasts only a short duration and varies across embryos. Consequently, sufficient high-quality samples of such intermediate stages is difficult to obtain in practice [3]. This intrinsic scarcity, coupled with privacy limitations in reproductive medicine, makes TLI data a prototypical small and imbalanced medical dataset.

To address the limitations of data availability, generative modeling has emerged as a promising solution for medical image augmentation. In particular, Generative Adversarial Networks (GANs) [4]–[8] have demonstrated strong capability in learning the underlying visual distribution and synthesizing realistic images. However, while GANs achieve stable and high-quality results on large-scale datasets, their training stability and generative quality are highly challenged under limited data conditions, which is precisely the case for TLI datasets. Specifically, a GAN uses a generator to transform noise from a Gaussian distribution into an image. Like most other generative models, the training goal of a GAN is to model the mapping from a well-sampled distribution (a Gaussian distribution) to a target training dataset (normally, a difficult-to-train distribution). While other generative models often have their own theoretical foundations and set the learning objectives for the generator based on this theory, a GAN uses a separate neural network—the discriminator—to learn the generator's training objectives.

# II. R3GAN vs. GANS

Recently, a special type of GAN called R3GAN [9] was proposed to combine the RpGAN [10] loss function with a unique gradient penalty (GP) loss function called zerocentered gradient penalties [11], [12]. Reference [11] conducted a rigorous mathematical derivation and ultimately demonstrated that, under reasonable assumptions, the combination of the RpGAN loss function and the zerocentered gradient penalty possesses a guarantee of local convergence. Architecturally, the GAN network is based on the ConvNeXt frontier convolutional network. The experiments of [9] show that R3GAN achieves comparable FID scores to diffusion models in both FFHQ and lowresolution ImageNet image generation. This study investigates the training dynamics of an R3GAN model—a refined residual-based GAN architecture—when applied to medical datasets, in particular, human embryo TLI images in this work. By analyzing the model's performance under large versus small data regimes, we aim to identify effective

strategies for improving generative quality in data-scarce medical applications.

# A. Traditional GAN Training Challenges and R3GAN Improvements

One of the most common challenges in training traditional GANs is instability and non-convergence. As GANs are inherently formulated as a minimax game between the generator and discriminator, their gradients often oscillate or diverge, making it difficult to reach equilibrium. The standard GAN loss forces the discriminator to separate real and fake samples, but in practice, this design encourages the generator to merely push samples across the decision boundary, leading to unstable gradient directions and distorted learning dynamics. R3GAN addresses this problem by extending the Relativistic Pairing GAN (RpGAN) framework with R1 and R2 zero-centered gradient penalties, which regularize the discriminator's gradients around zero. This addition effectively suppresses gradient explosion and provides a theoretically proven local convergence guarantee, resulting in significantly more stable adversarial training

A second major issue is mode collapse. In traditional GANs, the discriminator only compares isolated real and fake samples, creating an energy landscape with many poor local minima where the generator collapses to a few limited modes of the data distribution. RpGAN reformulates this interaction into a *relative comparison* between real and fake samples, such that each real sample defines a local decision boundary. This **pairwise loss** design prevents all samples from being pushed toward a single decision surface, allowing the generator to learn multiple modes and achieve better distribution coverage. Consequently, R3GAN achieves both stable training and improved diversity, with reduced KL divergence and Fréchet Inception Distance (FID) [13] compared to prior GAN variants.

Finally, traditional GAN training tends to rely heavily on heuristic techniques—such as minibatch standard deviation, specific weight initialization, and normalization tricks. These empirical methods may temporarily improve stability or sample diversity but lack theoretical justification and are difficult to generalize across architectures. R3GAN eliminates the dependence on such *ad-hoc* adjustments by integrating theoretically grounded regularization into its loss design. With this formulation, the model achieves superior stability and fidelity without external training tricks, and its framework generalizes naturally to modern backbones such as ResNet [14]. Overall, R3GAN demonstrates that a well-regularized, theoretically consistent loss function can replace manual tuning while improving convergence and generative quality.

# B. R3GAN Training Configuration and Dynamics on Large-Scale Datasets

Before discussing the small-scale training behavior in the next chapter, it is necessary to clarify several fundamental conventions and hyperparameters in R3GAN. The unit **kimg** refers to one thousand images processed during training, including both real and generated samples. This convention allows progress to be expressed independently of batch size or dataset scale, providing a consistent measure across different experiments.

A critical concept in R3GAN's training design is the **burn-in phase**, an early stage during which all major

hyperparameters—learning rate, R1/R2 regularization strength ( $\gamma$ ), Adam  $\beta_2$ , EMA half-life, and augmentation probability—are gradually transitioned from their initial to final values following a cosine schedule. The purpose of burnin is to allow the generator and discriminator to reach a balanced state before introducing full regularization. A large initial  $\gamma$  helps smooth both model distributions early in training, while the optimizer's low initial  $\beta_2$  enables rapid adaptation to changing gradient magnitudes. Meanwhile, augmentation is disabled at the start and progressively enabled only when the discriminator begins to overfit.

For large-scale datasets such as FFHQ 256×256 and ImageNet, R3GAN employs a short burn-in duration (8–20% of total training) and a rapid cosine decay of  $\gamma$  (e.g., 150  $\rightarrow$  15). These choices rely on the statistical stability of massive datasets, where diverse and abundant samples prevent overfitting and allow the discriminator to learn stable boundaries early. Consequently, aggressive hyperparameter decay accelerates convergence and reduces computational cost.

During large-scale experiments, R3GAN demonstrates fast initial convergence followed by a stable equilibrium, as evidenced by rapidly decreasing FID scores within the first few hundred kimg and steady improvement thereafter. The relativistic loss and zero-centered gradient penalties effectively suppress gradient explosion and mode collapse, while the cosine-scheduled burn-in ensures smooth transitions between early exploration and late refinement. Overall, the large-scale training configuration establishes the foundation from which this study explores alternative strategies for **small datasets**, where limited diversity and high gradient variance fundamentally alter these dynamics.

#### III. METHOD: TRAINING STRATEGY

This section describes the progressive development of a stable training strategy for R3GAN on the small-scale human embryo time-lapse imaging (TLI) dataset provided by Taichung Veterans General Hospital (TCVGH), comprising approximately 3.6k images.

The goal was to adapt the original large-dataset configuration of R3GAN to a data-constrained environment, where conventional training led to high FID values and unstable loss dynamics. Through a series of controlled experiments (exps 003–017), our investigation primarily focused on the **burn-in phase** and the  $\gamma$  **parameter controlling the R1 and R2 regularizations**, as these components are central to the R3GAN design.

Only representative experiments (exps 003–017) are presented below, while intermediate trials with overlapping settings are omitted for clarity. Note that the experiments are not necessarily discussed in sequential order, as each subsection focuses on the configurations that led to distinct observations.

# A. Original Baseline and Burn-in Exploration

Because the embryo dataset in this study most closely matches the FFHQ-256×256 setting in the original R3GAN paper, all images were resized to 256×256 and we first adopted a configuration similar to FFHQ-256 to enable fair comparison. To accommodate the small-dataset regime, the total training length was fixed at **300 kimg**, and we systematically varied the burn-in duration.

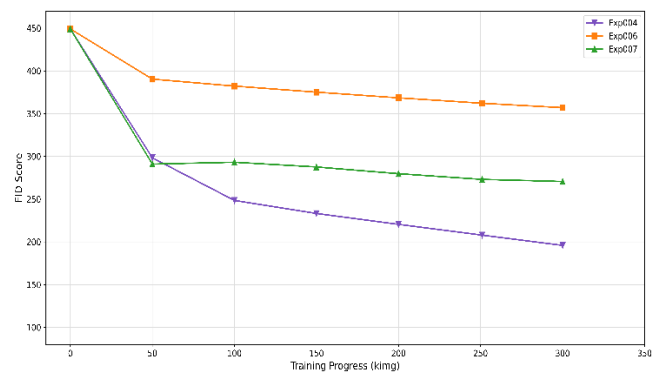


Fig. 1. FID Score comparison of three kinds of burn-in strategy.

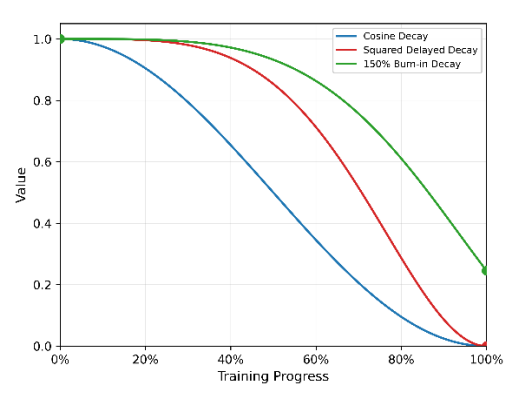


Fig. 2. Three kinds of decay strategy (assuming the parameter starts at 1 and decays to 0).

In the original R3GAN experiments, burn-in typically spans 8–20% of total training. Following this, exp 006 used a 20% burn-in, but performance was poor, with the best FID remaining above **250**. We then tested longer warm-ups: **exp 007 with 50% burn-in** and **exp 004 with 100% burn-in** (Fig. 1). Both outperformed the 20% baseline, and the 100% configuration (exp 004) was better than the 50% configuration (exp 007).

These results indicate that short burn-in schedules are unsuitable for small datasets. Since a small dataset provides limited learning signal, an overly short burn-in unduly compresses the model's effective learning time and pushes training prematurely into a late-stage, low-update regime, leading to under-training. Therefore, subsequent experiments adopted the 100% burn-in strategy.

# B. Delayed-Decay Scheduling

In earlier experiments, **exp 003** directly followed the FFHQ-256 training configuration from the original R3GAN paper, except that the total training length was shortened to **300 kimg**. Because its burn-in duration still corresponded to the original **2 Mimg** schedule used for large datasets, the hyperparameters effectively remained constant throughout training without any decay. Interestingly, this configuration achieved a rapid initial FID drop to **106**, outperforming exps 004, 006, and 007, although the FID later rebounded during the final stage.

Comparing both patterns revealed a clear trade-off: maintaining high hyperparameter values (i.e., little or no decay) allows a deeper initial FID drop but leads to later degradation, while enforcing a smooth, continuously decaying schedule ensures stable convergence but limits early improvement. To combine the advantages of both behaviors, we introduced a delayed-decay schedule—a curve that retains

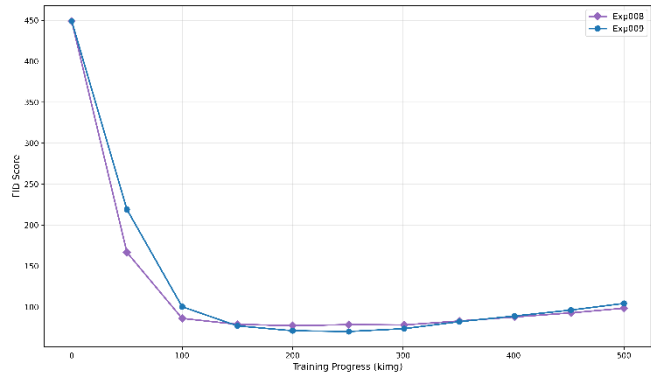


Fig. 3. FID comparison between exp008 and exp009.

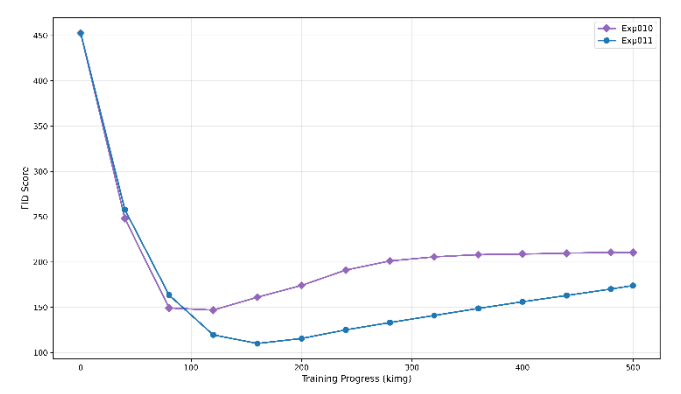


Fig. 4. FID comparison between exp0010 and exp011.

high hyperparameter values during the early phase and gradually decays toward the end. The cosine decay function used in R3GAN is given by  $0.5(1 + \cos(\pi x))$  (as shown by the blue line in Fig. 2), and by squaring the x-axis term, a "flattened head, steep tail" decay can be produced (red line in Fig. 2). An alternative delayed-decay strategy is to extend the burn-in phase to 150%, which similarly delays the onset of decay (green line in Fig. 2).

These two approaches correspond to **exp 008** (squared-decay schedule) and **exp 009** (150% burn-in). Exp 008 achieved a major improvement with a best FID of **77**, showing smoother late-stage behavior than exp 003. Exp 009 further reduced the FID to **70**, slightly outperforming 008. However, when comparing the two curves (Fig. 3), exp 009 showed weaker early and late performance, with only a marginal midphase advantage.

To verify that this difference was not due to random variation, two additional trials with different random seeds were performed (**exp 010** and **011**). As shown in Fig. 4, the overall pattern remained consistent—while some fluctuation existed, the **150% burn-in strategy (011)** still outperformed the squared-decay schedule (010). We therefore conclude that retaining stronger hyperparameter values in the early phase benefits small-dataset training, with extended burn-in offering a more reliable implementation of this principle.

# C. Reversing the $\gamma$ Schedule

In the original FFHQ-256 configuration, R3GAN employed a 20 % burn-in and a rapid  $\gamma$  decay (from  $150 \rightarrow 15$ ). This schedule worked well for large datasets, where tens of thousands of samples provide low-variance gradients, allowing the discriminator to establish a stable decision boundary early without overfitting. A short burn-in accelerates convergence and reduces training cost. However, for small datasets (e.g., only 3.6 k images), statistical noise

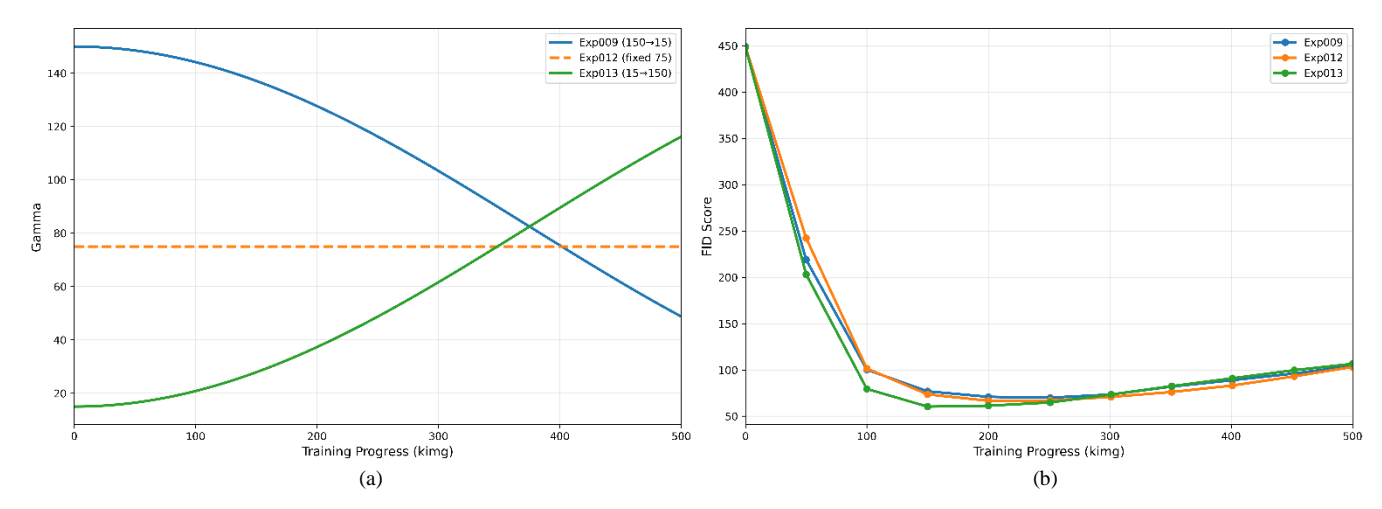


Fig. 5. Comparison of different γ scheduling strategies (exp009, exp012, and exp013). (a) γ variation during training. (b) Corresponding FID score trajectories.

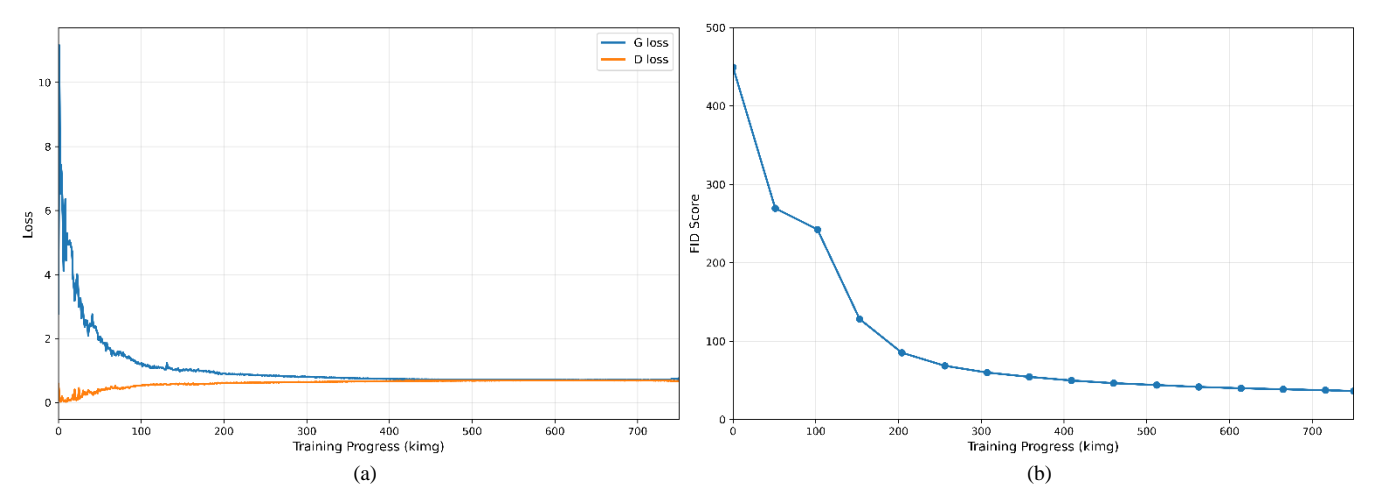


Fig. 6. Final training performance of exp017. (a) Generator and discriminator loss curves. (b) Corresponding FID score progression over 750 kimg.

amplified and batch diversity is limited. As a result, the discriminator tends to memorize the training samples within the first 20 % of training and becomes overly confident. If  $\gamma$  is then rapidly reduced—thus weakening the regularization—the discriminator overwhelms the generator, producing step-like FID oscillations and late-stage rebounds.

Re-examining the R1/R2 regularization design reveals that its purpose is to suppress the discriminator's gradient magnitude, preventing it from driving the generator away from equilibrium. Yet as training progresses, the generator should gradually approach equilibrium, implying that  $\gamma$  should increase rather than decrease in the later phase. Moreover, small datasets are prone to overfitting near the end of training and thus require stronger regularization support from  $\gamma$ .

To verify this hypothesis, we tested two reversed  $\gamma$  schedules: a **fixed**  $\gamma = 75$  setting (**exp 012**) and a **increasing schedule 15**  $\rightarrow$  **150** (**exp 013**). Compared to exp009, both configurations reduce regularization strength in the early stage and strengthen it later, while the latter applies a broader and more aggressive adjustment. Exp 012 surpassed the previous best (exp 009) with a minimum FID of **66.7**, and exp 013 further improved performance to **60.0**. When comparing the three strategies—**decreasing**  $\gamma$ , **fixed**  $\gamma$ , and **increasing**  $\gamma$ —(see Fig. 5), the increasing- $\gamma$  setup (exp 013) achieved a noticeable lead in the early phase and comparable stability in the later phase. These results support the small-to-large  $\gamma$ 

strategy, highlighting the distinct training requirements between small and large datasets.

Consequently, all subsequent experiments adopted the increasing  $\gamma$  schedule as the default configuration.

#### D. Lowering the y Range and Extending Training

As shown in Fig. 5, lower  $\gamma$  values in the early phase consistently produced better FID scores. This observation suggests that, for small datasets of this scale, a generally weaker regularization may help the generator retain richer gradient information and avoid early over-constraining. To validate this, we reduced the overall  $\gamma$  range by half—7  $\rightarrow$  75—and increased the late-stage augmentation probability to counter potential overfitting. This configuration was tested in **exp 014**.

Exp 014 achieved a new record FID of 57, and for the first time, the FID curve showed a steady downward trend until the end of training. The loss curves also exhibited no divergence compared to exp013, indicating that the original R3GAN  $\gamma$  range, which was optimized for large datasets, was indeed too high for this smaller domain.

Since FID was still decreasing at the end of 500 kimg, subsequent experiments extended the total training length to **750 kimg** and further reduced  $\gamma$  to explore its lower limit.

Through this process, the final configuration, exp017 ( $\gamma = 5 \rightarrow 40$ ), produced exceptionally smooth loss curves and reached an FID of **36** (see Fig. 6), demonstrating the strong potential of this low- $\gamma$  strategy for small datasets. Further reduction of  $\gamma$  did not yield any noticeable improvement.

From the baseline exp 006, which strictly followed the original FFHQ-256 configuration (20 % burn-in,  $\gamma=150 \rightarrow 15$ ), the training initially suffered from discriminator dominance, unstable adversarial balance, and a plateaued FID around 259. Through a series of targeted adjustments—extending the burn-in period, introducing delayed-decay schedules, reversing the  $\gamma$  trend, and finally lowering the overall  $\gamma$  range with extended training—the model achieved steady improvement in both stability and generative quality. The final **exp 017** configuration (burn-in = 150 %,  $\gamma$  = 5  $\rightarrow$  40,  $p_{aug} = 0 \rightarrow 0.6$ , 750 kimg) reached an **FID of 36**, marking an **86** % **reduction** relative to the baseline and completely eliminating the oscillatory FID patterns observed in earlier exps.

These results confirm that, compared to similar large-scale datasets, small-scale training benefits more from a longer burn-in phase, delayed and increasing  $\gamma$  scheduling, and a reduced overall regularization magnitude, which are key to maintaining stable adversarial dynamics and achieving sustained improvements in generative performance.

### IV. EXPERIMENTAL RESULTS

#### A. Qualitative Result

Before presenting the classification results, we first provide a qualitative demonstration of the images generated by the final configuration (exp017,  $\gamma = 5 \rightarrow 40$ ). Fig. 7 illustrates representative samples synthesized under this configuration, showing that the model successfully produces realistic and morphologically consistent embryo images. These examples are included solely for visual reference to verify the perceptual fidelity of the generator before downstream analysis.

#### B. Quantitative Comparison of Classification Results

To evaluate the effect of dataset balancing on model performance, we employed a BLIP-based [15] classifier. The BLIP (Bootstrapped Language—Image Pretraining) framework integrates a Vision Transformer (ViT) [16] as the visual encoder and a BERT-based text encoder [17] within a shared embedding space, enabling effective cross-modal alignment between visual and linguistic representations. This characteristic aligns well with the clinical workflow of

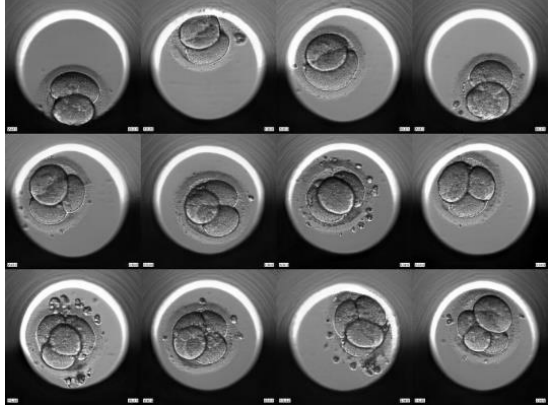


Fig. 7. Qualitative result of the final (exp017) configuration. The first, second, and third rows correspond to the t2, t3, and t4 developmental stages, respectively.

embryologists, who typically examine embryo morphology and then articulate their assessments through descriptive terms. By leveraging BLIP's inherent capability to associate images with textual semantics, our classifier can better simulate this interpretative process, potentially improving stage discrimination in subtle or transient developmental phases.

In this experiment, the classifier was first trained on the original unbalanced dataset, which contained 3101, 1164, and 3185 images for the two-cell (t2), three-cell (t3), and four-cell (t4) stage classes, respectively. The t3 class was therefore severely underrepresented, accounting for less than one-third of the samples in the other two classes. To mitigate this imbalance, approximately 2000 additional t3 images were generated using R3GAN with the exp017 configuration. These synthetic samples were then incorporated into the training set, resulting in a balanced dataset with roughly 3100 images per class. The classifier was retrained on this balanced dataset, and its performance was compared with the baseline model trained on the original data.

The quantitative comparison before and after dataset balancing is summarized in TABLE I. . Before balancing, the classifier exhibited extremely poor recognition of the t3 stage, with a recall of only 0.06 and an F1-score of 0.11. This result indicates that the model failed to capture the morphological patterns of t3 and almost never classified any image as belonging to this stage. After incorporating R3GAN-generated samples for data balancing, the recall of t3 dramatically increased to 0.69, and its F1-score improved from 0.11 to 0.60, indicating that the additional synthetic samples effectively enhanced the model's ability to identify this stage.

As shown in TABLE II., the recall of t4 slightly decreased after balancing, whereas its precision increased, resulting in an **unchanged** F1-score of 0.85. This mild trade-off is likely due to the model becoming more selective in predicting t4, reducing false positives while maintaining overall accuracy. The final F1-score did not decline, indicating that the model retained its ability to distinguish t4 effectively. The t2 metrics remained consistently high in both conditions, reflecting stable recognition of early cleavage stages. Overall, dataset balancing led to a more even classification performance across all classes.

In addition, the macro-averaged precision, recall, and F1-score all improved after balancing, increasing from 0.68 to 0.80~(+17.6%),~0.63 to 0.82~(+30.2%),~and 0.65 to 0.81~(+24.6%),~respectively. These results confirm that R3GAN-based augmentation improved the classifier 's overall balance among classes.

TABLE I. CALSSIFCATION METRICS BEFORE DATA BALANCING

Category	<b>Precision</b> ↑	Recall↑	F1-score↑
t2	0.97	0.99	0.98
t3	0.80	0.06	0.11
t4	0.74	0.99	0.85

TABLE II. CALSSIFCATION METRICS AFTER DATA BALANCING

Category	<b>Precision</b> ↑	Recall↑	F1-score↑
t2	0.96	0.96	0.96
t3	0.52	0.69	0.60
t4	0.91	0.80	0.85

Hardware: CPU/ AMD EPYC 7763 64-Core Processor with NVIDIA GPU/H100 and RAM/64 GB.

Software: Linux Ubuntu 24.04.1 LTS, Python 3.12.3, Cuda 12.4, cuDNN 9.1.0, PyTorch 2.6.0.

#### V. CONCLUTION

This study addresses the challenge of limited and imbalanced medical image datasets, a persistent obstacle in developing reliable machine learning systems for clinical applications. Using human embryo time-lapse imaging (TLI) as an example, we explored how generative adversarial networks (GANs) can be effectively trained under small-data conditions to produce realistic and diagnostically meaningful images.

Building upon the R3GAN framework, we conducted a series of controlled experiments to analyze the influence of key hyperparameters, such as burn-in phase length and  $\gamma$  regularization schedules. Through these experiments, we established a set of effective training strategies and, based on them, designed an optimized R3GAN configuration specifically tailored for 256×256-resolution datasets. This configuration (exp017), characterized by a full burn-in phase and a low, gradually increasing  $\gamma$  range (5  $\rightarrow$  40), achieved stable convergence and produced high-quality generated images suitable for downstream medical image analysis.

The generated samples successfully captured the morphological characteristics of different developmental stages (t2, t3, and t4), demonstrating the capability of the optimized R3GAN to augment small embryo datasets. By incorporating approximately 2000 generated t3 images into the training set, we balanced the dataset and retrained a BLIP-based classifier. The results showed that t3 recognition significantly improved—recall increased from 0.06 to 0.69, and F1-score from 0.11 to 0.60—while maintaining comparable performance in other classes. These findings verify that the proposed R3GAN training strategy can effectively mitigate data scarcity, enhance classification balance, and improve model robustness in small medical imaging datasets.

Overall, this work provides a practical reference for adapting GAN-based generative models to limited medical data. Future work will extend this approach to larger and more diverse embryo datasets, and explore multi-stage generative frameworks that jointly optimize image synthesis and clinical classification performance.

#### REFERENCES

 U.S. Congress, Health Insurance Portability and Accountability Act of 1996 (HIPAA), Public Law 104–191, 110 Stat. 1936, Aug. 21, 1996.
 [Online]. Available: https://www.hhs.gov/hipaa/

- [2] European Union, Regulation (EU) 2016/679 of the European Parliament and of the Council (General Data Protection Regulation, GDPR), Apr. 27, 2016. [Online]. Available: <a href="https://eur-lex.europa.eu/eli/reg/2016/679/oj">https://eur-lex.europa.eu/eli/reg/2016/679/oj</a>
- [3] J.-H. Wang, C.-H. Wu, M.-J. Chen, Y.-C. Yi, H.-W. Chang, and R.-Y. Wu, "EM-aided federated learning for quality assessment of embryo development," in *Proc. 2025 IEEE Int. Conf. Omni-layer Intell. Syst.* (COINS), Madison, WI, USA, 2025, pp. 1–6, doi: 10.1109/COINS65080.2025.11125796.
- [4] I. J. Goodfellow, J. Pouget-Abadie, M. Mirza, B. Xu, D. Warde-Farley, S. Ozair, A. Courville, and Y. Bengio, "Generative adversarial nets," in *Proc. 27th Int. Conf. Neural Inf. Process. Syst. (NeurIPS)*, Montreal, QC, Canada, Dec. 8–13, 2014, pp. 2672–2680.
- [5] A. Radford, L. Metz, and S. Chintala, "Unsupervised representation learning with deep convolutional generative adversarial networks," arXiv preprint arXiv:1511.06434, Jan. 2016.
- [6] M. Mirza and S. Osindero, "Conditional generative adversarial nets," arXiv preprint arXiv:1411.1784, Nov. 2014.
- [7] M. Arjovsky, S. Chintala, and L. Bottou, "Wasserstein generative adversarial networks," in *Proc. 34th Int. Conf. Mach. Learn. (ICML)*, Sydney, Australia, Aug. 6–11, 2017, pp. 214–223.
- [8] T. Karras, S. Laine, and T. Aila, "A style-based generator architecture for generative adversarial networks," in *Proc. IEEE/CVF Conf. Comput. Vis. Pattern Recognit. (CVPR)*, Long Beach, CA, USA, Jun. 16–20, 2019, pp. 4401–4410, doi: 10.1109/CVPR.2019.00453.
- [9] H. Y. Huang, A. Gokaslan, V. Kuleshov, and J. Tompkin, "The GAN is dead; long live the GAN! A modern GAN baseline," in *Proc. 38th Conf. Neural Inf. Process. Syst. (NeurIPS)*, Vancouver, Canada, 2024.
- [10] A. Jolicoeur-Martineau, "The relativistic discriminator: a key element missing from standard GANs," in *Proc. 7th Int. Conf. Learn. Representations (ICLR)*, New Orleans, LA, USA, May 6–9, 2019. [Online]. Available: <a href="https://arxiv.org/abs/1807.00734">https://arxiv.org/abs/1807.00734</a>
- [11] L. Mescheder, A. Geiger, and S. Nowozin, "Which training methods for GANs do actually converge?," in *Proc. 35th Int. Conf. Mach. Learn.* (ICML), vol. 80, Jul. 2018, pp. 3481–3490.
- [12] K. Roth, A. Lucchi, S. Nowozin, and T. Hofmann, "Stabilizing training of generative adversarial networks through regularization," in *Advances in Neural Information Processing Systems 30 (NeurIPS* 2017), Long Beach, CA, USA, Dec. 4–9, 2017, pp. 2019–2029.
- [13] M. Heusel, H. Ramsauer, T. Unterthiner, B. Nessler, and S. Hochreiter, "GANs trained by a two time-scale update rule converge to a local Nash equilibrium," in *Advances in Neural Information Processing Systems* 30 (NeurIPS 2017), Long Beach, CA, USA, Dec. 4–9, 2017, pp. 6626– 6637.
- [14] K. He, X. Zhang, S. Ren, and J. Sun, "Deep residual learning for image recognition," in *Proc. IEEE Conf. Comput. Vis. Pattern Recognit.* (CVPR), Las Vegas, NV, USA, Jun. 27–30, 2016, pp. 770–778, doi: 10.1109/CVPR.2016.90.
- [15] J. Li, D. Li, C. Li, and K. Keutzer, "BLIP: Bootstrapped languageimage pre-training for unified vision-language understanding and generation," in *Proc. Int. Conf. Mach. Learn. (ICML)*, Baltimore, MD, USA, Jul. 2022, pp. 12888–12900.
- [16] A. Dosovitskiy et al., "An image is worth 16×16 words: Transformers for image recognition at scale," in *Proc. Int. Conf. Learn. Representations (ICLR)*, Virtual Conf., May 3–7, 2021.
- [17] J. Devlin, M.-W. Chang, K. Lee, and K. Toutanova, "BERT: Pretraining of deep bidirectional transformers for language understanding," in *Proc. Conf. North American Chapter Assoc. Comput. Linguistics: Human Language Technologies (NAACL-HLT)*, Minneapolis, MN, USA, Jun. 2–7, 2019, pp. 4171–4186.